FISEVIER

Contents lists available at ScienceDirect

Journal of Molecular Liquids

journal homepage: www.elsevier.com/locate/molliq



Molecular dynamics simulation of steady-state droplet condensation on a fiber in direct contact membrane distillation settings



Saqlain Raza, Jixiong He, Hooman V. Tafreshi, Jun Liu*

Department of Mechanical and Aerospace Engineering, North Carolina State University, Raleigh, NC 27695, United States

ARTICLE INFO

Article history:
Received 29 September 2022
Revised 27 October 2022
Accepted 31 October 2022
Available online 4 November 2022

Keywords:
Molecular dynamics simulation
Direct contact membrane distillation
Desalination
Evaporation modelling
Condensation modelling
Steady-state evaporation
Droplet condensation

ABSTRACT

Understanding the dynamics of droplet condensation-evaporation behavior on fibers is important for improving the performance of fibrous membranes that are used in water purification applications, e.g., Direct Contact Membrane Distillation (DCMD). DCMD is a promising method of purifying water when low-grade waste heat or renewable energies are available. However, DCMD suffers from low throughput mass flux, and it is also prone to membrane flooding. We used molecular dynamics simulations in this work as the conventional (experimental or computational) methods do not have the required atomistic resolution to reveal the dynamics of water condensation-evaporation on the surface of fibers. Our simulations indicate that vapor flux across the membrane remains constant (with no droplet formation on the fiber) when the fibers' Young-Laplace Contact Angle (YLCA) is greater than a critical value at which condensation is suppressed. However, mass flux decreases with time at lower YLCAs due to the formation and growth of water droplets on the fibers, which could ultimately lead to membrane flooding. We also studied the impact of feed temperature, permeate temperature, fiber diameter, fiber position, and domain size on the fiber critical YLCA. Optimizing these parameters allows the use of a wide array of materials in membrane fabrication, including even hydrophilic materials, while preventing membrane flooding and also enhancing mass flux. In this work, we also present a novel methodology to simulate steady-state droplet condensation-evaporation process in the framework of molecular dynamics simulation, i.e., simulation times $>\sim 10$ ns, in contrast to the quasi-steady-state simulations (simulation time $<\sim 2$ ns) reported in most previous studies. Our work demonstrates a simulation platform to study the dynamics of the water condensation-evaporation on fibers and can be used to guide the design of DCMD membranes.

© 2022 Elsevier B.V. All rights reserved.

1. Introduction

Availability of safe water is critically important for public health, whether it is being used for drinking or other domestic purposes.[1] Generating fresh water from seawater, groundwater, or wastewater can be done using water desalination processes, where common techniques, such as reverse osmosis, multi-effect distillation, and multi-stage flash, are quite energy intensive.[2] Minimizing energy consumption or ensuring utilization of low-grade waste heat or renewable energy is considerably important to make the water accessible to regions lacking the necessary infrastructure.

Membrane distillation can harvest low-grade waste heat or renewable energy, which is a promising technique at the waterenergy nexus. It also has a higher salt rejection rate and requires lower hydraulic pressure compared to conventional water genera-

* Corresponding author. E-mail address: jliu38@ncsu.edu (J. Liu). tion techniques.[3,4] Fig. 1a shows this process, where impure feed water at high temperature evaporates and water vapor passes through a hydrophobic membrane to condense on the cold permeate side.[5] The hydrophobicity of the membrane prevents liquid water to pass through. Moreover, non-volatile solutes remain in the feed liquid stream as they are rejected by the liquid-vapor interface. The membrane distillation process has four main configurations: Direct Contact Membrane Distillation (DCMD), air gap membrane distillation, sweeping gas membrane distillation, and vacuum membrane distillation. DCMD is the simplest of all the configurations, therefore this work focuses on understanding, evaluating, and improving this process despite its lowest efficiency of four. Fig. 1b shows the three heat transfer steps in the DCMD process: convective heat transfer from the feed solution surface across the boundary layer to the membrane surface, heat transfer across the membrane by conduction, and convective heat transfer from the membrane surface to the bulk permeate side. [6,7].

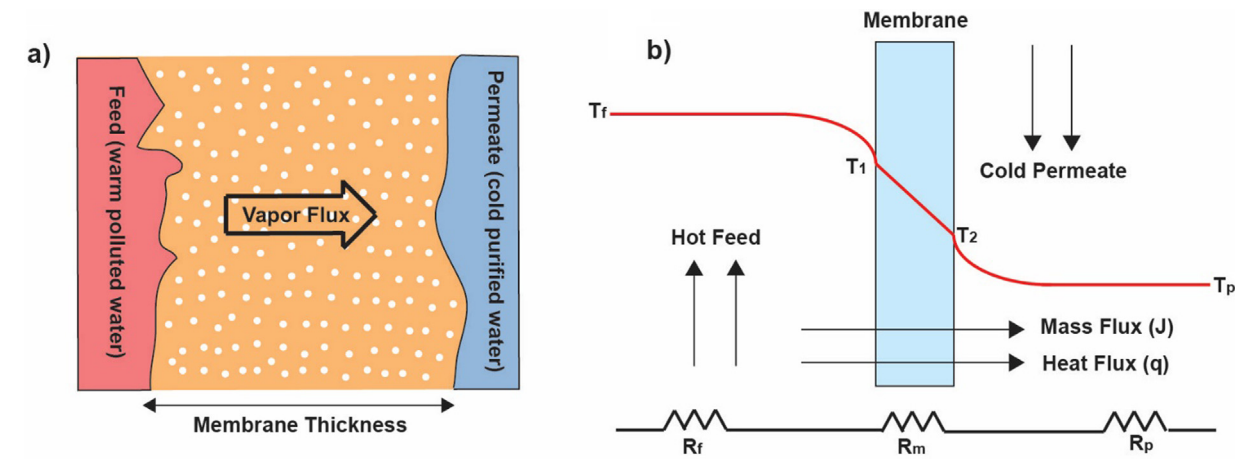


Fig. 1. (a) Mass transfer in the DCMD process. (b) Heat transfer in the DCMD process.

The DCMD method has been studied extensively over the past decade. Despite providing numerous advantages, this technique has not been scaled up for large industrial and domestic applications. This is primarily due to the low mass flux achieved via this process. Studies have indicated that the inefficiencies in the DMCD process are due to membrane inherent properties (e.g., Young-Laplace Contact Angle (YLCA), θ), geometrical parameters of the membrane, and process parameters.[8–15] Gradual wetting of the membrane coupled with fouling results in throughput decreasing over time. To prevent this, membranes with large porosity, ultra-thin thickness, high hydrophobicity, small pore size, and tortuosity are preferred, which in turn limits the membrane design.

Both experimental and computational methodologies have been used to optimize the DCMD parameters. Experimental techniques provide the benefit of analyzing the process in real-time but current techniques are not able to observe the water evaporation–condensation dynamics inside the membrane.[12] Computational techniques often characterize vapor transport through a membrane by assuming a straight cylindrical pore. [13,16–18] However, predetermined empirical factors are required for this molecular diffusion approach that is unique for each case, which impacts the feasibility of using this technique by increasing complexity.[19].

To overcome the limitations imposed by experimental and macroscale computational techniques, the molecular dynamics simulation technique has been used in this work to simulate vapor transport through a membrane. Molecular dynamics is an atomicscale computational technique that can be used to understand vapor condensation on the membrane fiber which can contribute to membrane flooding. Visualizing this phenomenon is extremely difficult using any other technique due to the challenges involved in imaging the vapor inside a DCMD membrane during operation. Furthermore, this technique can be used to understand and analyze the DCMD process including membrane properties, geometric parameters, and operating parameters. Developing a simulation method that closely depicts the actual process, would allow optimization of the membrane properties, geometric configurations, and operating conditions without requiring any empirical factors, and determining their impact on the enhancement of the mass flux.

Because of these advantages, there are a few molecular dynamics simulation studies in the past decade on the dependence of the DCMD process on membrane properties and process conditions. [20–23] For example, Hemeda et al. performed a qualitative analysis of the DCMD process using molecular dynamics simulations to demonstrate the impact of membrane dimensions, and temper-

ature difference between feed and permeate sides on the mass flux. [20] They concluded that the results from the simulations follow the trends of the actual process, and the molecular dynamics simulation can be used to optimize the DCMD process rather than trial and error. All the molecular dynamics simulations carried out for understanding the DCMD process consider membranes with high hydrophobicity and no relationship has been defined for the impact of hydrophobicity on the performance of the process. Moreover, the impact of feed temperature (T_p) , temperature difference (ΔT) , temperature gradient, and position of fiber on water condensation on the membrane is unclear.

In this work, the impact of membrane hydrophobicity on vapor transport, droplet condensation, and mass flux has been explored. It is presumably known that the DCMD process requires a membrane with high hydrophobicity. Understanding the phenomenon that prevents the use of hydrophilic membranes for the DCMD process and defining an optimum minimum YLCA would ensure the utilization of a wide array of materials. YLCA is defined as the contact angle of a certain liquid on a particular solid, and is dependent on the liquid surface tension, solid surface energy, and solid-liquid interfacial energy. Considering the interaction of water with a particular solid surface, the solid is considered hydrophilic (high wetting) if the YLCA < 90° and it is considered hydrophobic if the YLCA > 90°. For the sake of simplicity, a single fiber has been considered in our simulation while fiber hydrophobicity, position, and process temperatures have been varied to fundamentally understand the process.

In the remainder of this paper, we first describe the molecular dynamics simulation approach and methodology in **Section 2**, followed by the results of the simulations and discussion in **Section 3**. Finally, the conclusions drawn from our simulations are presented in **Section 4**.

2. Molecular dynamics simulation model and methods

2.1. Simulation domain and setup

In molecular dynamics simulations, trajectories of atoms are determined by numerically solving Newton's equations of motion for a model system of interacting particles.[24,25] After the position and velocity of these particles are initialized, each particle of the simulation system is updated using the velocity Verlet algorithm, and system properties including temperature, pressure, and energy are calculated based on statistical mechanics.[26] We used the open-source software package LAMMPS for our simulations due to its flexibility and proven accuracy.[27].

Fig. 2a represents the domain created in our simulations, which is a rectangular block with height H = 22.4 nm, width W = 6.7 nm, and length L = 20.1 nm. Periodic boundary conditions were applied in the x and z directions, whereas a fixed boundary condition was applied in the y-direction. The feed substrate at the bottom and the permeate substrate at the top consist of three regions each. The first layer, which is the thinnest of all, is fixed to act as a boundary for the simulation domain. The second layer acts as the heat source (or sink) with its temperature fixed using the Langevin thermostat. The third layer is designated as the free layer that interacts with water molecules and transfers heat (feed side) or absorbs heat (permeate side). Such configuration of the substrates, which has been adopted from the literature, is important for maintaining the stability of the system.[20,28] Moreover, this configuration makes sure that the system represents the actual DCMD process, in which the water is heated from an external heat source.

The interactions between different particles in molecular dynamics simulations are defined via interatomic potential functions. In this work, we have used well-defined potential functions that can accurately describe the behavior of actual substances. To depict the actual process, water, air, a feed substrate, a permeate substrate, and a fiber have been considered in the domain. For modeling the interactions between the water molecules, the SPC/

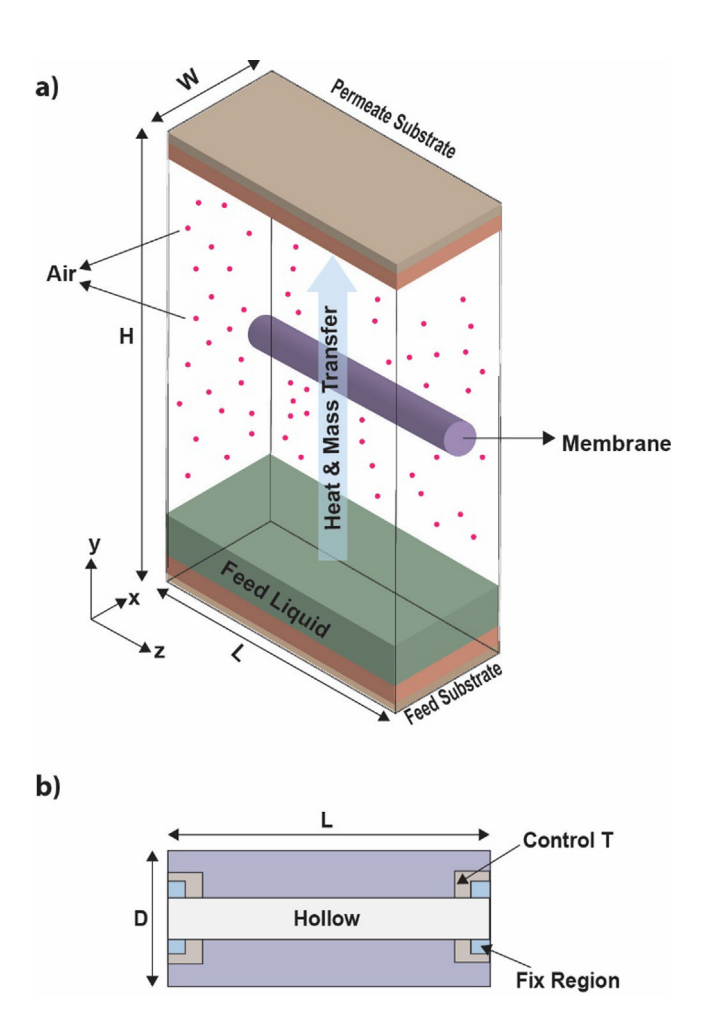


Fig. 2. (a) Simulation domain with a single fiber in the middle. The feed and permeate substrates consist of multiple layers to maintain the stability of the system. **(b)** Tri-layer structure of the fiber with inner sections at two ends fixed (blue color), middle sections at two ends set at a constant temperature (brown color), and outer section free to interact with water and/or air (purple color). The diameter of the fiber is D. (For interpretation of the references to color in this figure legend, the reader is referred to the web version of this article.)

E atomistic water model is considered due to its proven accuracy in predicting the physical properties such as density, surface tension, and evaporation enthalpy. [29] For simplicity, it was assumed that air consisted only of nitrogen as the molecular weight of air is almost the same as that of bi-atomic nitrogen gas, and it is simulated using the Pea model for its computational efficiency.[30] Using this model, air particles were considered as single Lennard-Jones (LJ) spheres with parameters σ = 3.75 Å and ϵ = 0.189 Kcal/mol. The interactions for the fiber particles, feed substrate, and permeate substrate were defined using the traditional LJ potential with parameters σ = 2.27 Å and ε = 9.44 Kcal/mol. [31,32] Similarly, the interactions between two different molecules (e.g., water and air, or water and fiber, etc.) were simulated using LI potential and the parameters for the equation were calculated based on Lorentz-Berthelot mixing rules.[33] The standard energy term in the LI potential equation is given as:

$$\epsilon_{ij} = \sqrt{\epsilon_i \epsilon_j},\tag{1}$$

The distance parameter in the equation is calculated as an arithmetic mean:

$$\sigma_{ij} = \frac{\sigma_i + \sigma_j}{2},\tag{2}$$

where i and j in equations (1) and (2) represent the two interacting molecules.

2.2. Modeling of membrane fiber

For simplicity, we have considered a single fiber that is placed in the middle of the simulation domain and extended along the entire length in the z-direction. Considering the computational challenge in modeling polymeric fibers due to their long chains, we assumed the fibers to be made of copper but with modified and realistic surface properties. When modeling the fiber in the membrane for molecular dynamics simulations, there are two requirements to ensure that the atomic-level kinetic behavior of the fiber is realistic: (1) The fiber needs to be fixed at a certain height; (2) The surface atoms of the fiber are not fixed to ensure proper interactions with the liquid droplets, vapor, and air. If the inner portion of the fiber is fixed (typically done by removing the interaction forces or removing the velocity) to fix the location and the outer portion is unconstrained, the heat transfer will inevitably happen between the inner portion with 0 K temperature and the outer portion. In other words, the inner portion of the fiber acts as a heat sink at 0 K, which is unrealistic and will significantly decrease the surface temperature of the fiber. To avoid this simulation artifact, we modeled the fiber with a tri-layer structure with diameter D = 2 nm in the radial direction as shown in Fig. 2b: the inner layer, the middle layer, and the outer layer. The inner layer was fixed; the temperature of the middle layer was set at a constant temperature (based on the linear temperature profile of the simulation domain) using a Langevin thermostat; the outer layer is unconstrained. The inner and middle portions of the fiber were modeled only at the left and right ends, and not through the entire fiber length to have a minimum effect on the outer section. In this approach, the surface temperature of the fiber will be more realistic and follow the general temperature profile of the DCMD process while at the same time the fiber is fixed at the designated height. Furthermore, the fiber was designed to be atomically smooth by controlling the distance between atoms (proportional to the lattice spacing) to be less than the diameter of the water vapor molecule.

While significantly reducing the CPU time, these fibers made up of copper will depict the surface wetting behavior of the polymeric fibers via the modified Lorentz–Berthelot mixing rule which is given as [20,34,35]:

$$\epsilon_{ij} = r\sqrt{\epsilon_i \epsilon_j}. \tag{3}$$

The factor 'r' in equation (3) changes the surface wettability with water. The above relation and the values of 'r' were obtained from the literature and the values were verified for two contact angles of 120° and 90° on a flat surface. Although the dependence of θ on factor r was determined for a flat surface, the same YLCA is expected to be obtained on a cylindrical fiber as the Young-Laplace contact angle is a material property and is independent of the geometry of the surface considering that the surface roughness and heterogeneity are the same.[36].

2.3. Simulations for system relaxation and dynamics

The simulation timestep is set as 1 fs unless specified. The energy minimization of the simulation domain was performed after setting up the system followed by two equilibration runs: (1) The first microcanonical ensemble (constant number of molecules, volume, and energy - NVE) equilibration run was done for 150 ps where the inner layer of the feed and permeate substrates, and the inner portion of the fiber was fixed while the middle portion of fiber and substrates were heated to a temperature of 298 K using a Langevin thermostat. The water and air molecules were also heated to a temperature of 283 K using a Langevin thermostat. (2) The second NVE equilibration run was also done for 150 ps. The temperature profiles of the fiber and the substrates were kept the same with the inner section being fixed, a middle section at a temperature of 298 K, and the outer portion unconstrained. Different from the first run, the water and air molecules were kept unconstrained and allowed to reach equilibrium with other surfaces. After two equilibration runs, the simulation was run for 10 ns to probe the water dynamics. The fiber and substrates were kept in the NVE ensemble, and their inner sections were fixed. The middle sections of the feed substrate and permeate substrate were kept to a temperature of 363 K and 283 K respectively. The water and air molecules were again left unconstrained so that they could be heated or cooled by the interactions with the outer portions of the substrates or fiber.

2.4. Achieving a steady-state supply of water

During the simulation, as water evaporates from the feed side to the permeate side, the water level at the feed side would decrease with time and a final dry state would occur impacting the overall dynamics of the system, which deviates from the intent of this simulation. The concept of disjoining pressure defining the attractive force by the surface on fluid film is a well-established phenomenon, and it increases with a decrease in the thickness of the film. In our study, even before reaching the dry state, the film of liquid water on the feed side becomes thin, which would increase the disjoining pressure and decrease the evaporation rate.[37,38] This constraint needs to be removed by constantly adding water into the simulation domain, which mimics the real process. To our best knowledge, there are no simple solutions to resolve this issue. One commonly used method in the literature is to keep the running time of the simulation short so that a quasi-steady state is assumed where the decrease of the evaporation rate is not significant over a short period of time. [28,39] However, this method hinders the potential to evaluate the long-time process, for example, the water dynamics of evaporation and condensation. The other method is Grand Canonical Monte Carlo (GCMC) which has been widely used for studying diffusion at the atomic scale.[40-42] In the grand canonical ensemble, the Temperature T, the Volume V, and the chemical potential μ are held constant, whereas the number of molecules fluctuates. In this work, water molecules can be inserted on the feed side and deleted from the permeate side independently by applying separate GCMC ensembles with external reservoirs. However, due to its stochastic nature, it is extremely difficult to control the water molecules added and removed in the simulation domain especially in the presence of the fiber as it introduces additional resistance. Moreover, the GCMC method inserts water molecules in a gaseous state due to which they evaporate quickly impacting the overall dynamics of the system. Controlling the temperature of water molecules inserted in the simulation domain and equilibrating them with the already-present water was another challenge faced while using this technique.

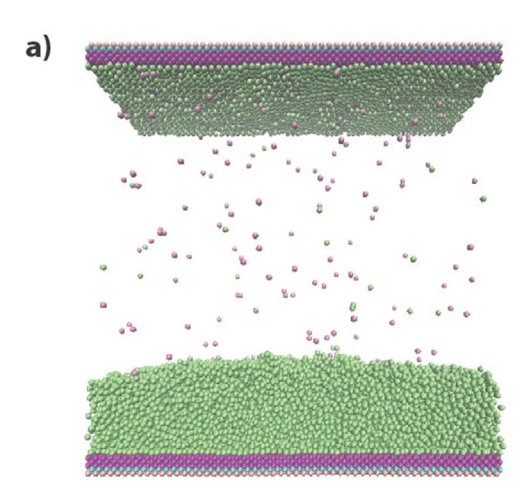
In this work, we have developed a methodology to add water molecules into the simulation domain with a defined frequency. We removed the condensed water from the permeate side and added differential water to the feed side using delete_atoms and create_atoms commands available in LAMMPS after every 0.5 ns. The frequency of adding water molecules needs to be adjusted based on different simulation systems and is generally dependent on the evaporation rate from the feed side. If the evaporation rate is too fast, water can be added at a higher frequency and vice versa. The basic concept is to ensure that added water is not more than 10 % of the water available, otherwise the temperature reduction in feed water is quite significant which will impact the evaporation rate. The differential water molecules were added randomly in a region created on the top of the already present feed water and they were defined in a separate group using their IDs. Moreover, to ensure that the added water molecules do not impact the dynamics of the system, we removed the added water molecules if they overlap with the current water molecules in the domain while keeping the location of the rest of the particles in the domain fixed during energy minimization. The added water was then heated to an average temperature of the simulation domain and the simulation was continued. A similar treatment was done on the permeate side. Using this methodology, the simulation can be run for an infinitely long time without affecting the stability of the system while at the same time achieving a constant supply and removal of water during the simulation. The methodology was verified using the simulation domain without the fiber, which will be discussed in the next section.

3. Results and discussion

In this section, we present the results of molecular dynamics simulations obtained for the DCMD process with fibers having different YLCAs. The impact of important operating parameters on the evaporation–condensation phenomenon in the system has also been presented.

3.1. Verification of the steady-state supply of water

First, the methodology for achieving a steady-state supply of water discussed in **Section 2.4** was tested for the simulation domain without any fiber as shown in Fig. 3a. Considering the evaporation–condensation dynamics, here the (net) mass transfer in the unit of mg/m² is calculated by counting the cumulative number of water molecules evaporating from the feed side and condensing on the permeate side. The mass flux (unit: mg/m²ns) is then defined as the first-order derivative of the mass transfer as a function of time, which is the slope on the mass transfertime plot. Fig. 3b shows that mass flux remains constant with small fluctuations in the case of a steady-state supply of water using our new methodology, termed in this work as the steady-state method. The same method was used to run the simulation for a longer time of 25 ns and a similar trend was observed throughout without any decay in the mass flux. On the contrary, the mass flux significantly



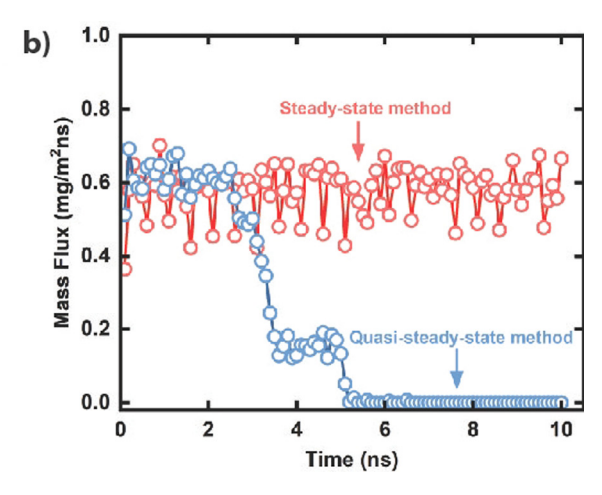


Fig. 3. (a) Evaporation-condensation dynamics without the fiber. The molecules shown in purple are air molecules and in green are water molecules. (b) Mass flux remains constant with fluctuations at every 0.5 ns for the steady-state method, whereas it decays significantly towards zero after 2 ns for the quasi-steady-state method. (For interpretation of the references to color in this figure legend, the reader is referred to the web version of this article.)

decreases after approximately 2 ns when the conventional method (termed as quasi-steady-state method) of using a fixed number of water molecules in the domain was used. These results agree with the general phenomenon of evaporation–condensation on a flat surface. The slight fluctuations in mass flux for the first case are due to the addition of water which is at a lower temperature (~323 K) in comparison with the already-present water in the simulation domain (~360 K). Due to this low temperature of the incoming water, the overall temperature of the water decreases resulting in a slightly decreasing value of mass flux. This cycle is repeated every 0.5 ns when the water is added to the simulation domain. The contrast in Fig. 3b verifies the steady-state supply of water in our simulations.

3.2. Impact of fiber hydrophobicity on mass transfer

We investigated the role of fiber hydrophobicity on the mass transfer in the membrane using the same technique to ensure a steady-state supply of water so that a long-time simulation of the evaporation-condensation dynamics of water on fiber can be observed. Several YLCAs were tested including 70°, 80°, 90°, 100°, and 120°. The feed temperature of 363 K and permeate temperature of 283 K were considered in these simulations. Fig. 4a shows that water condenses on the fiber and starts forming a droplet when $\theta \leq 90^{\circ}$ but no droplet is formed when $\theta \geq 100^{\circ}$. To understand the reasons for the decrease in mass flux at smaller YLCAs, the dynamic process visualized using the Visual Molecular Dynamics (VMD) software [43] indicates that for $\theta = 70^{\circ}$, 80°, and 90°, the water condensing on the fiber does not evaporate quickly and consequently starts forming a droplet on the fiber. As mentioned in **Section 2.1**, periodic boundary conditions are used in the x and z directions due to which a mirror image of the droplet can be seen (Fig. 4a(i) and 4a(iii)). Fig. 4b indicates that mass flux starts to decrease when $\theta \leq 90^\circ$ due to the droplet formation on the fiber whereas it remains constant when $\theta > 100^{\circ}$.

This droplet creates a barrier for the transfer of water evaporating from the feed side to condense on the permeate side. On the contrary, as the hydrophobicity of the fiber increases by increasing the YLCA to 100° or greater, there is no droplet formation on the fiber. Even though the water condenses on the fiber, it evaporates quickly to the permeate side. This phenomenon can be understood by the fact that water has a stronger interaction with the fiber at a smaller YLCA as indicated by the higher value of the r parameter. Due to the stronger interaction, the water molecules stay on the

fiber for enough time to transfer their energy to the fiber surface via heat conduction. As more water molecules condense on the fiber following the same phenomenon and release their energy, they form a thin water film on the fiber. With further condensation on the fiber after the formation of the film, water molecules start to form a droplet due to the strong interaction between them, and surface tension. Another important aspect to note is that water molecules initially condense on the bottom surface of the fiber and release their energy via heat conduction. With the remaining energy, they move to the top of the fiber but as the droplet grows in size, this motion becomes more difficult due to the greater distance between the bottom of the droplet and the top of the fiber surface.

To quantify the impact created by the presence of fiber and the creation of droplets, transport resistance (R) was calculated for all the YLCAs considered in this study. The transport resistance (R) can be mathematically given as [21]:

$$R = \frac{J_{e,f} - J_{e,p}}{I},\tag{4}$$

where J is the DCMD mass flux, $J_{e,p}$ and $J_{e,p}$ are the evaporation mass flux from the feed side and permeate side respectively. Since the evaporation from the permeate side is extremely small compared to the feed side, we can assume that $J_{e,p}$ is equal to zero, therefore the equation can be simplified as:

$$R = \frac{J_{ef}}{I},\tag{5}$$

Fig. 5 indicates that transport resistances for θ = 100° and 120° remain constant with only small fluctuations. The non-zero resistance for these YLCAs is only due to the presence of fiber. However, for the θ = 90°, 80°, and 70°, the transport resistances keep increasing due to the formation and growth of droplets on the fiber. This is again because, at a smaller YLCA, the interaction strength between fiber and water increases, and the droplet formation rate also increases.

3.3. Droplet growth on fiber

To understand what finally happens with droplets formed on the fiber, the simulation was kept running for a total time of 25 ns for θ = 70°. Fig. 6a visualizes this behavior and indicates that the droplet keeps growing and finally covers the entire surface of the fiber. This droplet formation and growth has an adverse effect

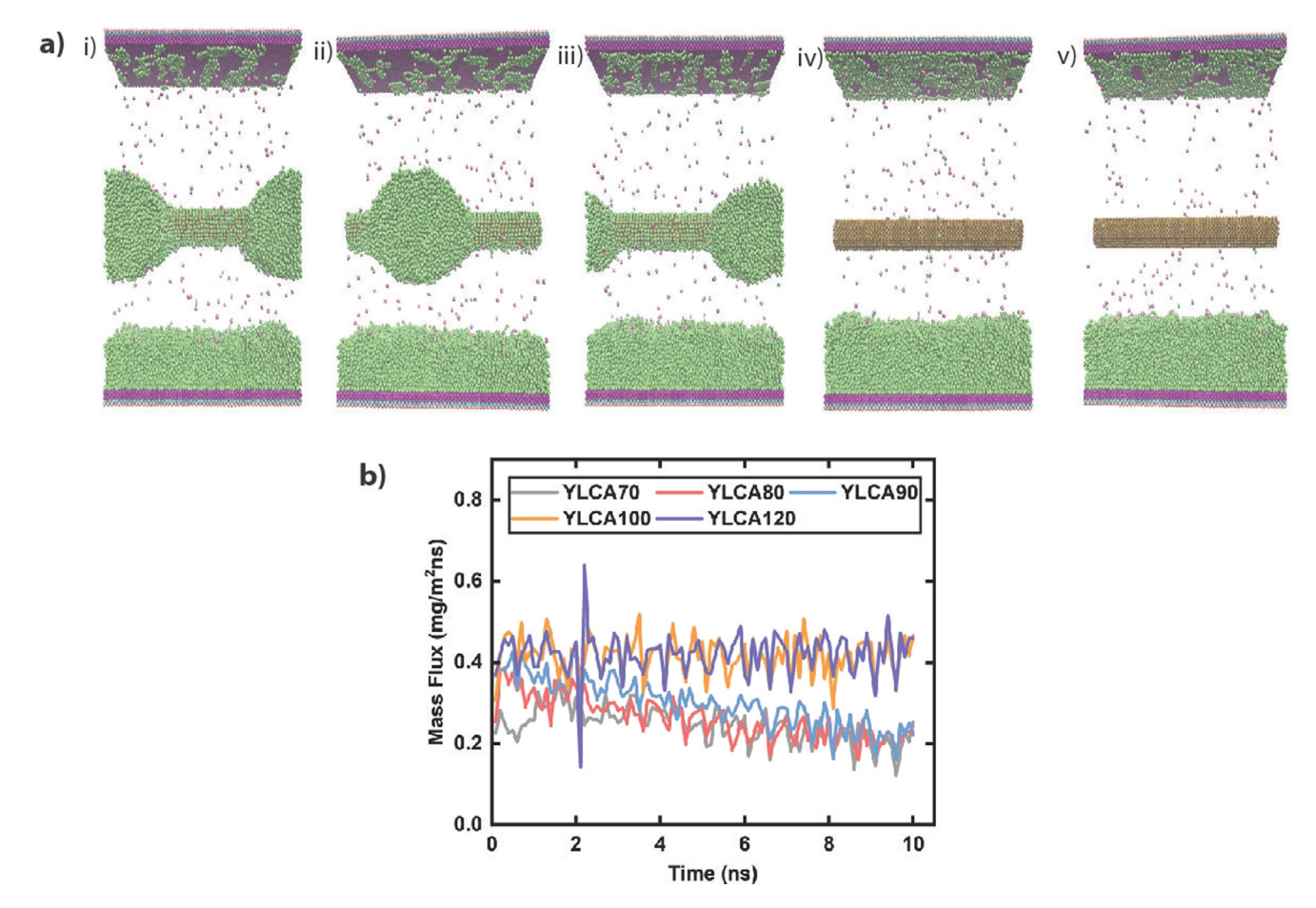


Fig. 4. Impact of YLCAs. (a) VMD snapshots at the simulation time t = 10 ns when the YLCAs (θ) are different (i) $\theta = 70^{\circ}$ (ii) $\theta = 80^{\circ}$ (iii) $\theta = 90^{\circ}$ (iv) $\theta = 100^{\circ}$ (v) $\theta = 120^{\circ}$. (b) Mass flux decreases with time when $\theta \le 90^{\circ}$ and it remains constant when $\theta \ge 100^{\circ}$.

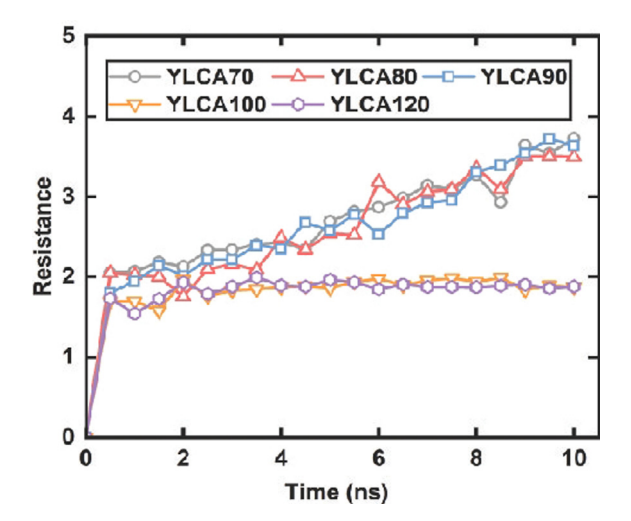


Fig. 5. Impact of YLCA on the transport resistance (R). The R remains constant when $\theta \geq 100^\circ$ as there is no droplet formation, however for $\theta \leq 90^\circ$, it keeps on increasing due to the droplet formation and growth on the fiber.

on the performance as shown by decreasing mass flux values in Fig. 6b, and it can ultimately lead to membrane flooding on the macroscale. Therefore, if the membrane is designed properly by considering the factors that impact the droplet formation on fibers, this condition can be minimized.

The rate of water transport from the feed side to the fiber is greater than that from the fiber to the permeate side due to which the droplet size keeps on increasing even after the droplet covers the entire surface of the fiber. However, the mass flux becomes constant as it is only being contributed by the evaporation of water from the fiber to the permeate side.

3.4. Factors affecting critical YLCA

Critical YLCA is the minimum contact angle at which water condensation on fiber is suppressed in the DCMD environment. Based on the simulation parameters in Sections 3.2-3.3 ($T_{\rm f}\approx 363$ K and $T_{\rm p}\approx 283$ K), the critical YLCA was determined to be $100^{\circ}.$ Feed temperature, permeate temperature, fiber diameter, simulation domain height, and position of the fiber are the major factors that might impact the value of critical YLCA. Mathematically, this can be given as:

$$\Theta_{cri} = f(T_f, T_p, d_f, H, z_f), \tag{6}$$

where, Θ_{cri} represents critical YLCA, T_f , T_p , d_f , H, and z_f represent feed temperature, permeate temperature, the diameter of the fiber, the height of the simulation domain, and the position of fiber respectively. In this work, we mostly evaluate the impact of T_f and T_p on the critical YLCA while briefly discussing the influence of fiber position, fiber diameter, and the height of the simulation domain. Table 1 represents the temperatures considered in this study. The temperature range for T_f was taken to be 323–363 K,

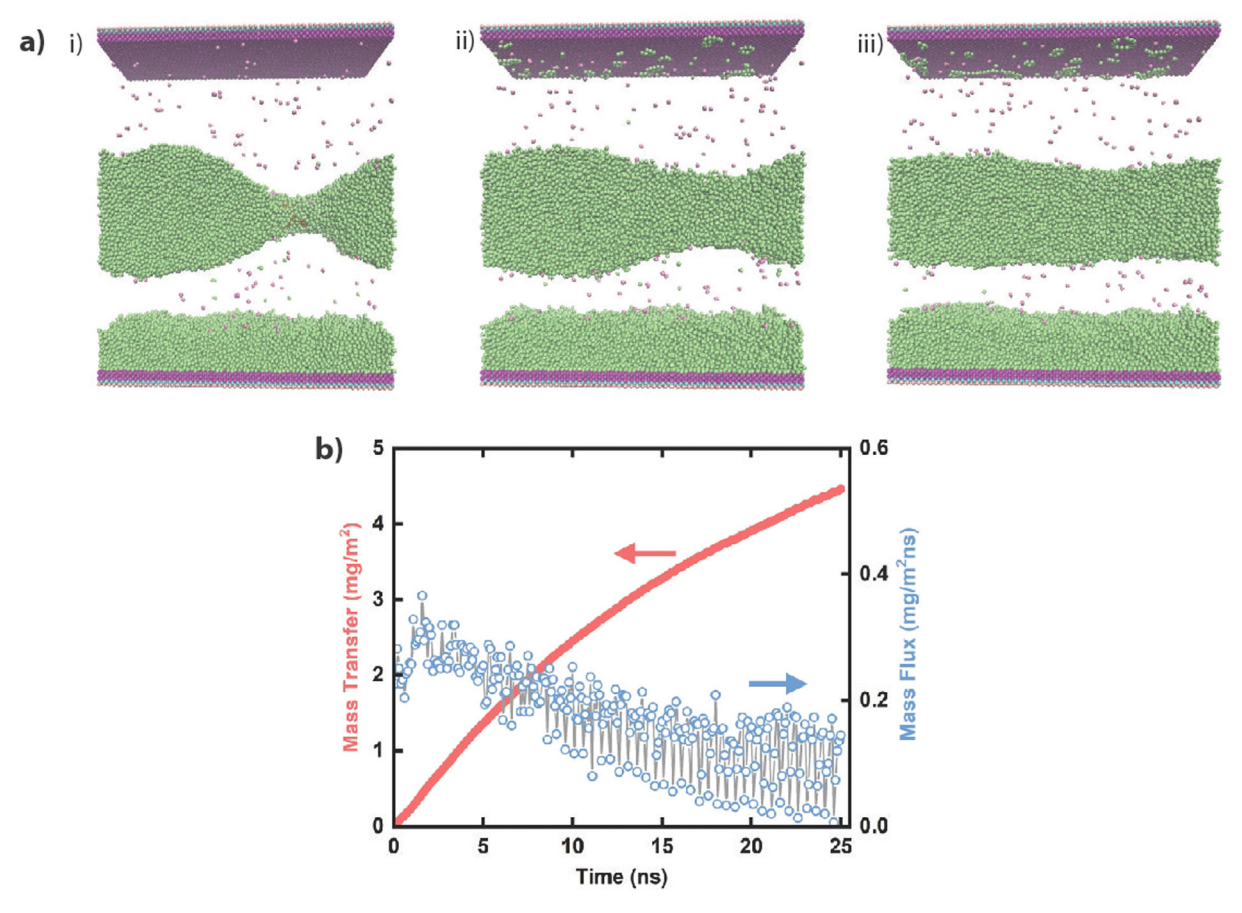


Fig. 6. (a) Droplet formation and growth at $\theta = 70^{\circ}$ at (i) t = 16.5 ns (ii) t = 16.7 ns (iii) t = 17 ns. (b) Mass transfer and mass flux for $\theta = 70^{\circ}$. Mass transfer decreases till 17 ns and then becomes linear. Similarly, mass flux also decreases till 17 ns and then becomes constant.

 $\label{eq:total_total_total} \textbf{Table 1} \\ \text{Feed temperatures, permeate temperatures, and associated temperature difference} \\ \text{for determining the critical YLCA. } \\ \Theta_{cri} \text{ increases with an increase in } \Delta T \text{ and } T_f.$

T _f (K)	T _p (K)	ΔT (K)	Critical YLCA
323	283	40	83
333	293	40	85
343	303	40	85
353	313	40	85
363	323	40	85
333	283	50	88
343	293	50	89
353	303	50	90
363	313	50	90
343	283	60	90
353	293	60	91
363	303	60	91
353	283	70	94
363	293	70	94
363	283	80	98

and that for $T_{\rm p}$ was taken to be 283–323 K. These temperature ranges are in agreement with the previous studies done for understanding DCMD process at the macroscale.

The simulation results shown in Fig. 7 are based on the simulation setup shown in Fig. 2a where the fiber is in the middle, which indicate that $\Theta_{\rm cri}$ has a strong dependence on ΔT . At a constant feed or permeate temperature, critical YLCA increases with an increase in ΔT . This is because as ΔT increases, the temperature difference across the fiber also increases allowing the water vapor to condense easily on the fiber at lower contact angles. Therefore, a material with higher hydrophobicity (lower wettability) will be

required as the ΔT increases. At a constant ΔT , the Θ_{cri} increases with an increase in feed temperature but the increase is not significant. The increase in Θ_{cri} can be explained by the fact that as ΔT is constant, the permeate temperature also increases and it becomes difficult for the water vapor to condense on the permeate side which is more elevated with an increase in water evaporating from the feed side due to greater feed temperature. The same is the case for the dependence of Θ_{cri} on permeate temperature at a constant ΔT . Furthermore, at a constant feed temperature, θ_{cri} decreases with an increase in permeate temperature as shown in Fig. 7b. The value of ΔT decreases with an increase in permeate temperature if the feed temperature remains constant. The temperature of the fiber also increases and prevents water vapor from condensing on the fiber surface resulting in a lower critical contact angle. Therefore, at a constant ΔT , fiber material with higher hydrophobicity will be required with an increase in T_f or T_p and at a constant T_f, material with higher wettability can be used with an increase in

Previous results indicate that increasing ΔT will increase the critical YLCA. This would result in a decrease in the material selection array for an efficient DCMD process. However, further analysis shown in Fig. 8 indicates that mass flux would increase with the increase in ΔT . Therefore, considering a lower ΔT for the less hydrophobicity requirement will result in the mass flux to decrease, and hence, there is a compromise between membrane hydrophobicity and mass flux.

In the previous results, we demonstrated the impact of ΔT on the critical YLCA while keeping the height of the simulation domain (H) constant. However, the temperature gradient that is the change in temperature over H should also be evaluated to

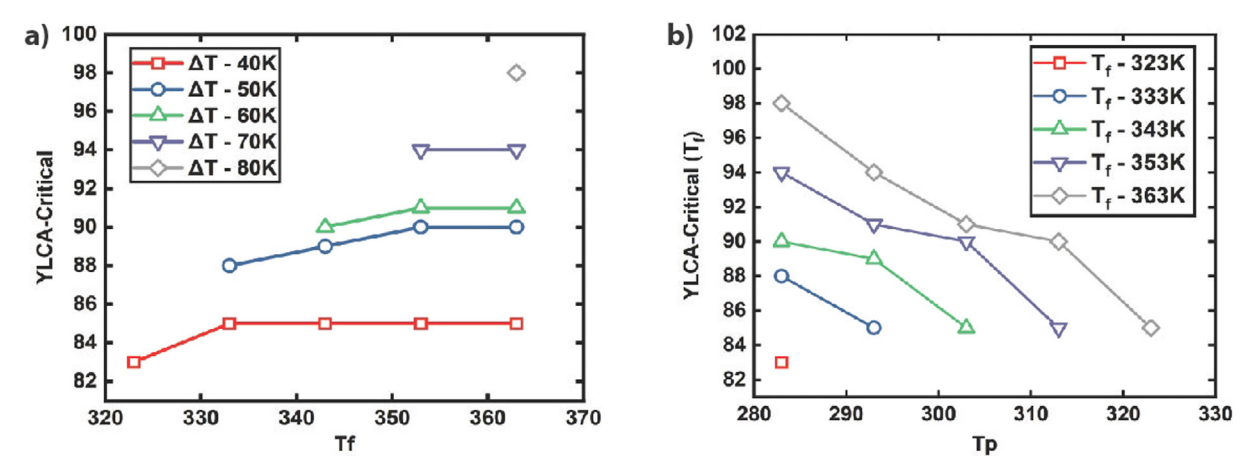


Fig. 7. (a) Impact of T_f on Θ_{cri} at a constant ΔT . (b) Impact of T_p on Θ_{cri} at a constant T_f .

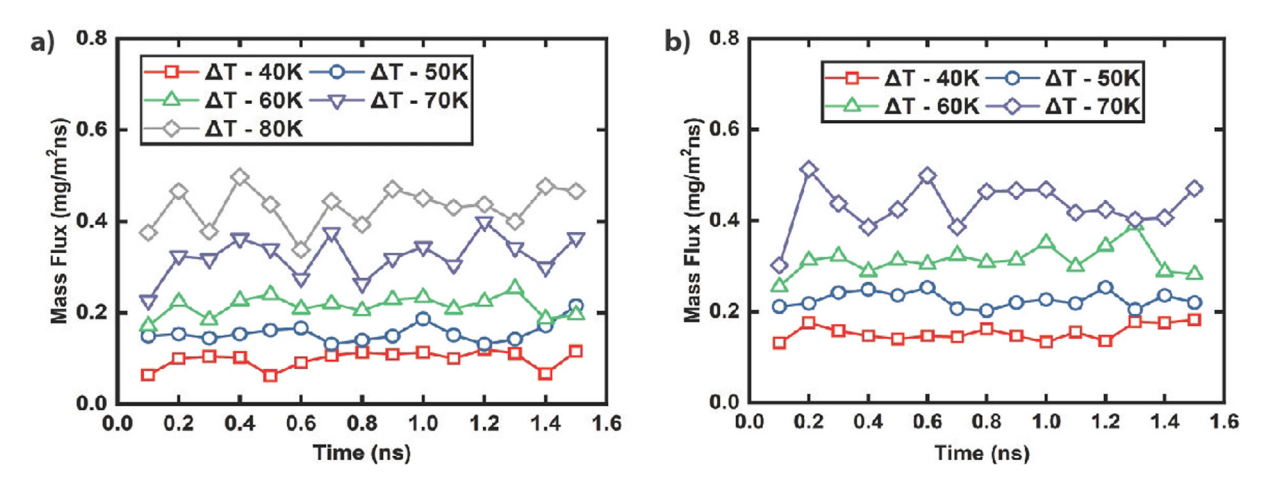


Fig. 8. (a) Increase in mass flux with ΔT at $T_p = 283$ K. (b) Increase in mass flux with ΔT at $T_p = 293$ K.

assess its impact on critical YLCA. Two cases were considered in which the temperature gradient was varied by considering 2H and H/2 as the height of the simulation domain but the ΔT was kept the same. Simulation domains with height H and H/2 are shown in Fig. 9. The results indicate that the critical YLCA is not dependent on the temperature gradient and only changes with ΔT . This is because the number of air molecules in the simulation domain also changes with the change in H due to which the temperature distribution of the fiber remains the same and hence, the water condensation-evaporation on the fiber follows the same trend. Since the evaporation-condensation rate at the fiber remains the same, Θ_{cri} shows no change with the increase or decrease in height of the simulation domain. Although, the Θ_{cri} remains the same but the change in temperature gradient by changing H impacts the mass flux. For the case when ΔT is 40 K and the temperature gradient is increased by reducing the height of the simulation domain to H/2, the mass flux at the critical YLCA increases, whereas it decreases when the temperature gradient is reduced by increasing the height of the simulation domain to 2H. This is because as the size of the simulation domain is halved, water molecules experience fewer collisions and take less time to reach the permeate side due to a smaller distance and hence the mass flux increases.

As mentioned in **Section 3.2**, water molecules condense on the bottom side of the fiber and release their energy via heat conduction. These water molecules translate to and evaporate from the top side of the fiber. Therefore, if the diameter of the fiber is

increased, the value of $\Theta_{\rm cri}$ might change as indicated by Equation (6), due to a greater distance between the bottom and top sides of the fiber. To explain the impact of fiber diameter on the critical YLCA, we evaluated the phenomenon with a fiber diameter of 2D (i.e., 4 nm) as shown in Fig. 10. The feed temperature of 363 K and permeate temperature of 283 K were considered for this variation. The results indicate that $\Theta_{\rm cri}$ increases from 98° to 101°, i.e., the fiber with a higher hydrophobicity is required, when the fiber diameter is doubled. Moreover, the mass flux reduces by increasing the diameter of the fiber due to a greater time required by the water molecules to evaporate from the fiber and reach the permeate side.

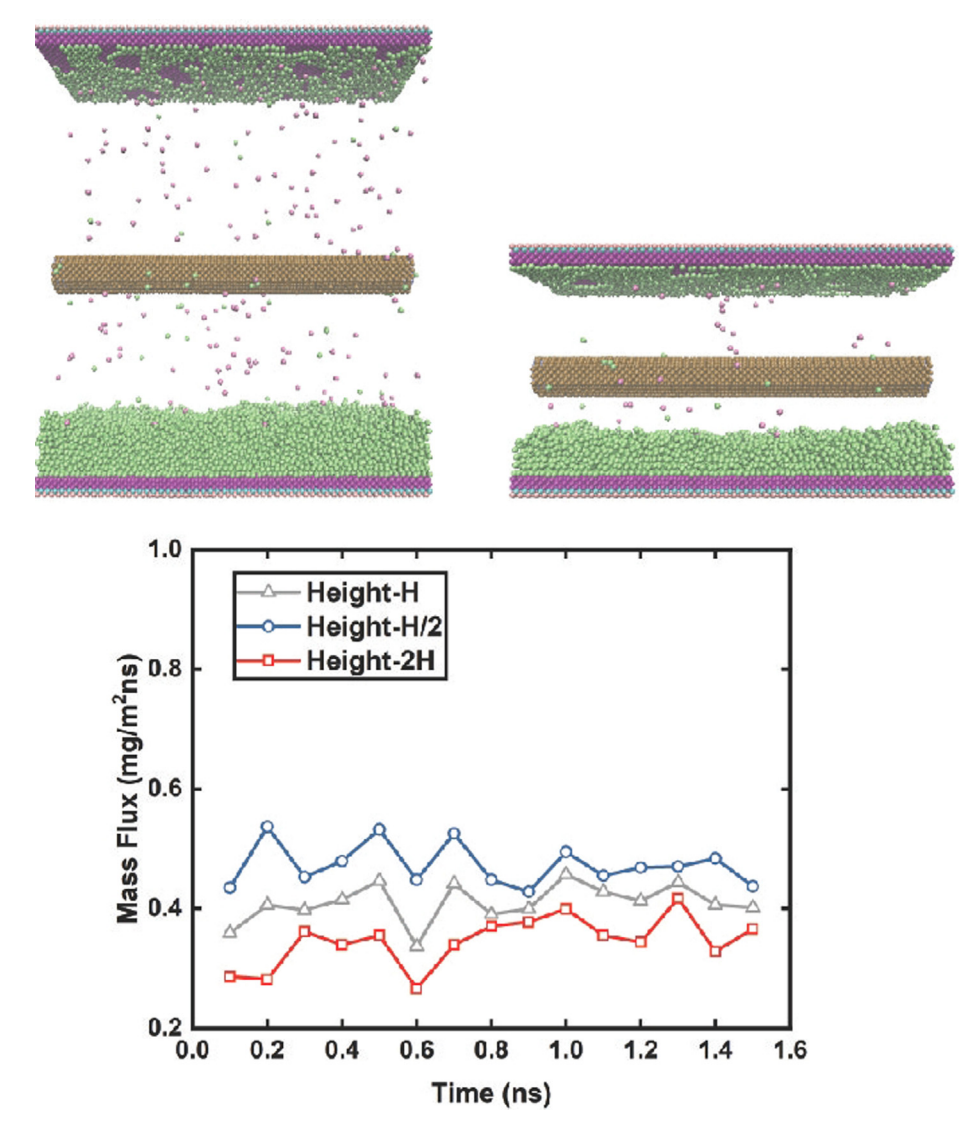


Fig. 9. Top panel: VMD snapshots of the simulation domains with the height of 2H (left) and H/2 (right), respectively. Bottom panel: Mass flux vs time for simulations with different domain heights (different temperature gradients).

molecules interacting with the fiber will have a relatively higher temperature due to fewer collisions with air molecules. This results in a decrease of $\theta_{\rm cri}$ in this case. Moreover, when the fiber is moved closer to the permeate side, the exact opposite trend is observed as the critical YLCA increases from 85° to 91°. These results clearly show that $\theta_{\rm cri}$ not only depends on ΔT but also has a strong dependence on the position of the fiber which should be considered when selecting the material for the membrane. However, at the critical YLCA, mass flux values remain the same regardless of the fiber position in the simulation domain.

3.5. Membrane design guidelines

Equation (6) evaluates the impact of factors including feed temperature (T_f) , permeate temperature (T_p) , fiber position (z_f) with respect to the feed and permeate sides, simulation domain height (H), and fiber diameter (d_f) on fiber hydrophobicity (Θ_{cri}) requirements. The simulation results indicate that Θ_{cri} is not dependent on the simulation domain height (H). However, optimizing other parameters would allow the use of hydrophilic materials for membrane fibers and membranes with hydrophobicity gradient across their thickness can help to enhance the efficiency of the DCMD pro-

cess. Following are the key design guidelines based on the simulation results:

- (i) Lowering ΔT (difference between feed and permeate temperatures) would allow the use of fiber materials with less hydrophobicity (lower YLCA). Although, this would reduce the mass flux values achieved from the process.
- (ii) Fibers closer to the feed side are less prone to droplet formation at the same contact angle. In other words, lower hydrophobic materials can be used for fibers close to the feed side and opposite is true for fibers closer to the permeate side.
- (iii) Increasing the diameter of the fiber increases the hydrophobicity requirement. Therefore, fibers with lower wettability will be required if the diameter of the fiber is increased.

4. Conclusions

This work presented here demonstrate the use of molecular dynamics simulations in improving the understanding of the DCMD process. Nanoscale phenomena such as water condensation and evaporation on a fiber as well as the dynamics of droplet for-

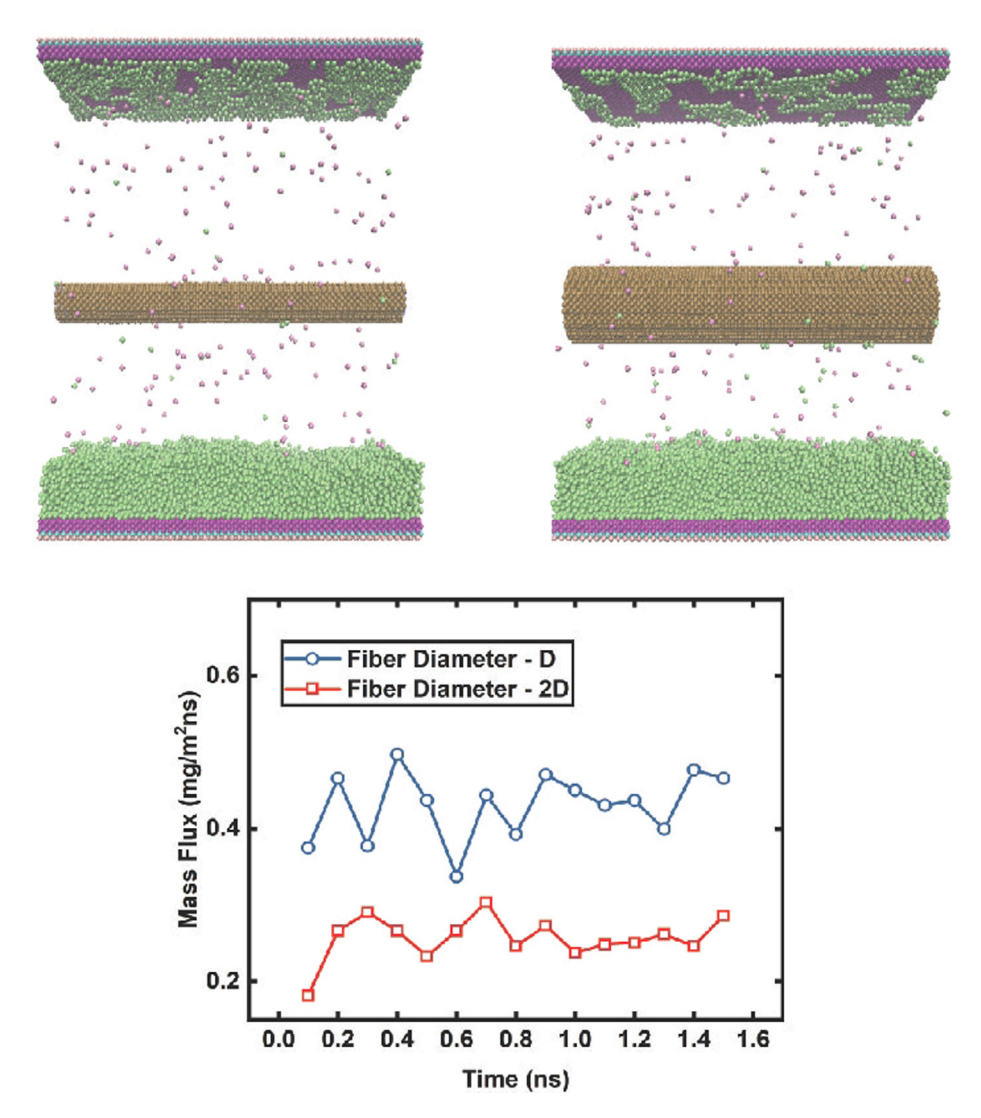


Fig. 10. Top panel: VMD snapshots of the simulation domains with the fiber diameter (d_f) of D (left) and 2D (right), respectively. Bottom panel: Mass flux vs time for simulations with different fiber diameters.

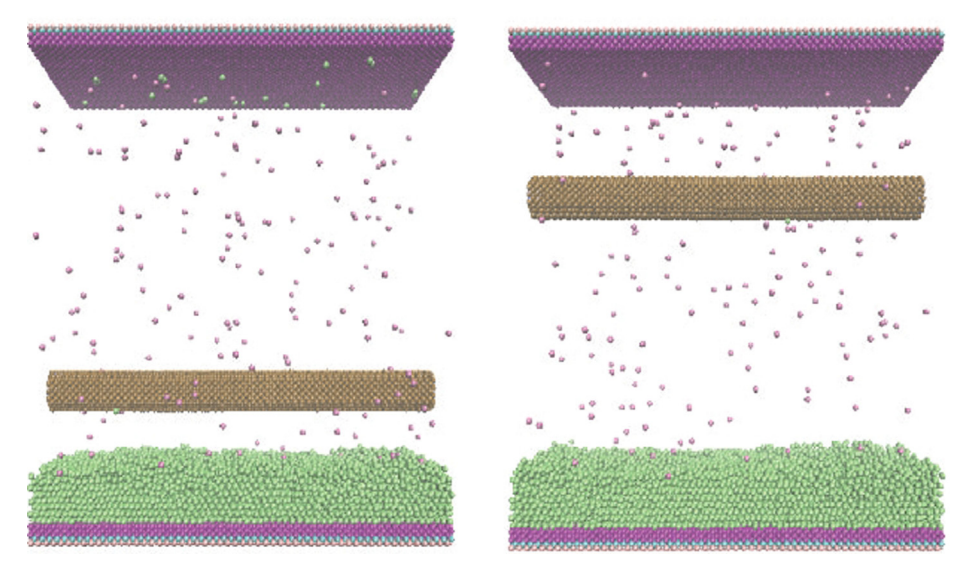


Fig. 11. Simulation domain with the fiber close to the feed side (left) and close to the permeate side (right).

mation and growth are studied in this paper. Our results indicate that droplet formation on the fibers can be prevented if the fibers are made of a material with an YLCA that is greater than a critical value. This allows the fibers to remain dry and allow water vapor to travel from the feed side to the permeate side with minimal resistance (i.e., maximum mass flux). On the other hand, when the fibers' YLCA is smaller than the above critical value, water droplets form on the fibers and consequently lower the rate of mass transfer across the membrane or lead to membrane flooding. Our simulation results indicate that Θ_{cri} depends strongly on ΔT amongst other factors such as feed and permeate temperatures, the fiber diameter, and the distance between the fiber and feed or permeate (increasing ΔT increases Θ_{cri}). However, for a given ΔT , Θ_{cri} was seen to increase with feed and permeate temperatures. In other words, less hydrophobic materials can be used for DCMD, when the temperature difference across the membrane is lower.

Although our simulations are on scales 3–4 orders of magnitude smaller than those of the actual process, the parameter assessment reported in this paper provides a guideline for selecting the most appropriate materials for the membrane. For instance, our simulations revealed that fibers closer to the feed side are more prone to droplet formation. Therefore, creating membranes having a hydrophobicity-gradient across their thickness can help to enhance the efficiency of the DCMD process.

CRediT authorship contribution statement

Saqlain Raza: Methodology, Software, Validation, Formal analysis, Investigation, Data curation, Writing – original draft. **Jixiong He:** Methodology, Software, Validation, Writing – review & editing. **Hooman V. Tafreshi:** Conceptualization, Writing – review & editing, Supervision. **Jun Liu:** Conceptualization, Methodology, Resources, Writing – review & editing, Supervision, Project administration.

Data availability

Data will be made available on request.

Declaration of Competing Interest

The authors declare that they have no known competing financial interests or personal relationships that could have appeared to influence the work reported in this paper.

Acknowledgements

Computational resources were provided by the High-Performance Computing Center at North Carolina State University and Extreme Science and Engineering Discovery Environment (XSEDE) which is supported by National Science Foundation grant number ACI- 1548562. S. R. is supported by the American Chemical Society Petroleum Research Fund New Direction Award and the NC State Research and Innovation Seed Funding (RISF). J. H. is supported by the National Science Foundation under the award number CBET 1943813.

References

- J.M. Hughes, J.P. Koplan, Saving lives through global safe water, Emerg. Infect. Dis. 11 (10) (2005) 1636.
- [2] A. Yadav, P.K. Labhasetwar, V.K. Shahi, Membrane distillation using low-grade energy for desalination: a review, J. Environ. Chem. Eng. 9 (2021).
- [3] A. Deshmukh, C. Boo, V. Karanikola, S. Lin, A.P. Straub, T. Tong, D.M. Warsinger, M. Elimelech, Membrane distillation at the water-energy nexus: limits, opportunities, and challenges, Energy Environ. Sci. 11 (5) (2018) 1177–1196.

- [4] R. Ullah, M. Khraisheh, R.J. Esteves, J.T. McLeskey Jr, M. AlGhouti, M. Gad-el-Hak, H.V. Tafreshi, Energy efficiency of direct contact membrane distillation, Desalination 433 (2018) 56–67.
- [5] S. Srisurichan, R. Jiraratananon, A.G. Fane, Mass transfer mechanisms and transport resistances in direct contact membrane distillation process, J. Membr. Sci. 277 (2006) 186–194.
- [6] J. Phattaranawik, R. Jiraratananon, A.G. Fane, Heat transport and membrane distillation coefficients in direct contact membrane distillation, J. Membr. Sci. 212 (2003) 177–193.
- [7] H. Chang, C.D. Ho, J.A. Hsu, Analysis of heat transfer coefficients in direct contact membrane distillation modules using CFD simulation, J. Appl. Sci. Eng. 19 (2016) 197–206.
- [8] F. Laganà, G. Barbieri, E. Drioli, Direct contact membrane distillation: modelling and concentration experiments, J. Membr. Sci. 166 (2000) 1–11.
- [9] M. Gryta, Fouling in direct contact membrane distillation process, J. Membr. Sci. 325 (2008) 383–394.
- [10] M. Khayet, A. Velázquez, J.I. Mengual, Modelling mass transport through a porous partition: Effect of pore size distribution, J. Non-Equilib. Thermodyn. 29 (2004) 279–299.
- [11] J. Phattaranawik, R. Jiraratananon, A.G. Fane, Effect of pore size distribution and air flux on mass transport in direct contact membrane distillation, J. Membr. Sci. 215 (2003) 75–85.
- [12] Y.M. Manawi, M. Khraisheh, A.K. Fard, F. Benyahia, S. Adham, Effect of operational parameters on distillate flux in direct contact membrane distillation (DCMD): comparison between experimental and model predicted performance, Desalination 336 (2014) 110–120.
- [13] M.S. El-Bourawi, Z. Ding, R. Ma, M. Khayet, A framework for better understanding membrane distillation separation process, J. Membr. Sci. 285 (2006) 4–29.
- [14] T.M. Bucher, B. Emami, H.V. Tafreshi, M. Gad-el-Hak, G.C. Tepper, Modeling resistance of nanofibrous superhydrophobic coatings to hydrostatic pressures: the role of microstructure, Phys. Fluids 24 (2) (2012).
- [15] B. Emami, H.V. Tafreshi, M. Gad-el-Hak, G.C. Tepper, Effect of fiber orientation on shape and stability of air-water interface on submerged superhydrophobic electrospun thin coatings, J. Appl. Phys. 111 (6) (2012).
- [16] A. Alkhudhiri, N. Darwish, N. Hilal, Membrane distillation: a comprehensive review, Desalination 287 (2012) 2–18.
- [17] J.G. Lee, W.S. Kim, J.S. Choi, N. Ghaffour, Y.D. Kim, Dynamic solar-powered multi-stage direct contact membrane distillation system: concept design, modeling and simulation, Desalination 435 (2018) 278–292.
- [18] A. Ali, J.H. Tsai, K.L. Tung, E. Drioli, F. Macedonio, Designing and optimization of continuous direct contact membrane distillation process, Desalination 426 (2018) 97–107.
- [19] M. Ghadiri, S. Fakhri, S. Shirazian, Modeling and CFD simulation of water desalination using nanoporous membrane contactors, Ind. Eng. Chem. Res. 52 (2013) 3490–3498.
- [20] A.A. Hemeda, R.J.A. Esteves, J.T. McLeskey Jr, M. Gad-el-Hak, M. Khraisheh, H.V. Tafreshi, Molecular dynamic simulations of fibrous distillation membranes, Int. Commun. Heat Mass Transfer 98 (2018) 304–309.
- [21] H. Zhang, B. Liu, H.T. Kieu, M.S. Wu, K. Zhou, A.W.K. Law, Coarse-grained molecular dynamics study of membrane distillation through meso-size graphene channels, J. Membr. Sci. 558 (2018) 34–44.
- [22] S. Pillai, A. Santana, R. Das, B.R. Shrestha, E. Manalastas, H. Mishra, A molecular to macro level assessment of direct contact membrane distillation for separating organics from water, J. Membr. Sci. 608 (2020).
- [23] S. Velioğlu, L. Han, J.W. Chew, Understanding membrane pore-wetting in the membrane distillation of oil emulsions via molecular dynamics simulations, J. Membr. Sci. 551 (2018) 76–84.
- [24] L. Martinez, R. Andrade, E.G. Birgin, J.M. Martínez, PACKMOL: A package for building initial configurations for molecular dynamics simulations. J. Comput. Chem. 30 (2009) 2157–2164.
- [25] S. Cheng, J.B. Lechman, S.J. Plimpton, G.S. Grest, Evaporation of Lennard-Jones fluids, J. Chem. Phys. 134 (2011).
- [26] N. Bou-Rabee, Time integrators for molecular dynamics, Entropy 16 (2014) 138–162.
- [27] in't Veld, P. J., Plimpton, S. J. & Grest, G. S. <u>Accurate and efficient methods for modeling colloidal mixtures in an explicit solvent using molecular dynamics</u>. Computer Physics Communications 179, 320–329, (2008).
- [28] E. Bird, J. Gutierrez Plascencia, P. Keblinski, Z. Liang, Molecular simulation of steady-state evaporation and condensation of water in air, Int. J. Heat Mass Transf. 184 (2022).
- [29] S. Chatterjee, P.G. Debenedetti, F.H. Stillinger, R.M. Lynden-Bell, A computational investigation of thermodynamics, structure, dynamics and solvation behavior in modified water models, J. Chem. Phys. 128 (2008).
- [30] B. Coasne, A. Galarneau, F. di Renzo, R.J.M. Pellenq, Molecular simulation of nitrogen adsorption in nanoporous silica, Langmuir 26 (2010) 10872– 10881
- [31] H.R. Seyf, Y. Zhang, Molecular dynamics simulation of normal and explosive boiling on nanostructured surface, J. Heat Transfer 135 (2013).
- [32] Y. Mao, Y. Zhang, Molecular dynamics simulation on rapid boiling of water on a hot copper plate, Appl. Therm. Eng. 62 (2014) 607–612.
- [33] J. Chen, J.-G. Mi, K.-Y. Chan, Comparison of different mixing rules for prediction of density and residual internal energy of binary and ternary Lennard-Jones mixtures, Fluid Phase Equilib. 178 (2001) 87–95.
- [34] J. Vrabec, J. Stoll, H. Hasse, Molecular models of unlike interactions in fluid mixtures, Mol. Simul. 31 (2005) 215–221.

- [35] D. Niu, G.H. Tang, The effect of surface wettability on water vapor condensation in nanoscale, Sci. Rep. 6 (2016) 1–6.
- [36] X.F. Wu, Y.A. Dzenis, Droplet on a fiber: Geometrical shape and contact angle, Acta Mech. 185 (2006) 215–225.
- [37] X. Wang, Y. Li, J.A. Malen, A.J.H. McGaughey, Assessing the impact of disjoining pressure on thin-film evaporation with atomistic simulation and kinetic theory, Appl. Phys. Lett. 116 (2020).
- [38] H. Hu, Y. Sun, Molecular dynamics simulations of disjoining pressure effect in ultra-thin water film on a metal surface, Appl. Phys. Lett. 103 (2013).
- [39] A. Chandra, P. Keblinski, Investigating the validity of Schrage relationships for water using molecular dynamics simulations, J. Chem. Phys. 153 (2020).
- [40] G.S. Heffelfinger, F. van Swol, Diffusion in Lennard-Jones fluids using dual control volume grand canonical molecular dynamics simulation (DCV-GCMD), J. Chem. Phys. 100 (1994) 7548–7552.
- [41] H. Frentrup, C. Avendaño, M. Horsch, A. Salih, E.A. Müller, Transport diffusivities of fluids in nanopores by non-equilibrium molecular dynamics simulation, Mol. Simul. 38 (2012) 540–553.
- [42] A. Rahbari, A. Poursaeidesfahani, A. Torres-Knoop, D. Dubbeldam, T.J.H. Vlugt, Chemical potentials of water, methanol, carbon dioxide and hydrogen sulphide at low temperatures using continuous fractional component Gibbs ensemble Monte Carlo, Mol. Simul. 44 (2018) 405–414.
- [43] W. Humphrey, A. Dalke, K. Schulten, VMD: visual molecular dynamics, J. Mol. Graph. 14 (1) (1996) 33–38.